MINISTRY OF INDUSTRY & TRADE
INDUSTRIAL UNIVERSITY OF HO CHI MINH CITY



HO VAN MINH HAI

SYNTHESIS, CHARACTERIZATION AND APPLICATION OF HIERARCHICAL STRUCTURED IRON OXIDE NANOCOMPOSITE MATERIAL

SUMMARY OF DOCTORATE THESIS

HO CHI MINH CITY, 2024

MINISTRY OF INDUSTRY & TRADE
INDUSTRIAL UNIVERSITY OF HO CHI MINH CITY

HO VAN MINH HAI

SYNTHESIS, CHARACTERIZATION AND APPLICATION OF HIERARCHICAL STRUCTURED IRON OXIDE NANOCOMPOSITE MATERIAL

SUMMARY OF DOCTORATE THESIS

Major: Chemical engineering

Code: 9520301

Independent reviewer 1:

Independent reviewer 2:

Reviewer 1: PGS.TS Đoàn Văn Đạt
Reviewer 2: TS Nguyễn Thành Danh
Reviewer 3: PGS.TS Đoàn Văn Hồng Thiện

SUPERVISOR

1. Prof. Nguyen Van Cuong
2. Prof. Vo The Ky

HO CHI MINH CITY, 2024

INTRODUCTION

1. Criticality

In the past decades, the development and application for nanomaterial have received much attention from domestic and international researches, due to their unique properties compared to bulk materials. Recent efforts have been focused on studying semiconductor metal oxide nanostructures to exploit their physical and chemical properties. Among recent research directions, the design of hierarchical semiconductor metal oxide nanostructures with uniform morphology, high surface area has been widely applied in various field, such as catalyst and sensors…can be considered an effective direction.

Iron oxide, a typical semiconductor metal oxide, has been of particular interest to many scientists for research in various fields. To date, there have been numberous in-depth studies on nanostructures iron oxide materials with hierarchical structures, due to their unique physicochemical properties that are not present in other metal oxides. The important factors that effect the physicochemical properties of nanostructured iron oxxide materials mainly originate from their multivalent states, as well as their dependence on morphology, surface effect, and particle size. Currently, many different hierarchical nanostructured iron oxide morphologies, such as rods, wires, sheets, hollow spheres have been synthesized using various methode, such as sol-gel, co-precipitation, hydrothermal, emulsion, and microwave method. To enhance the effectiveness of single-phase iron oxide applications, one of the feasible approach is to combine it with other components such as carbon material (graphene, carbon nanotubes, porous carbon,…), noble metals (Au, Ag, Pt,…), or other semiconductor metal oxide (Co_3O_4, NiO, MnO_2, ZnO…) to form hierarchical nanostructured nanocomposites. This combination often enhances the surface area, electrical conductivity, and physicochemical properties of the nanocomposites material compared to the single-phase material.

Although there have been many study, synthesis and application of various metal oxide nanocomposites as well as well hierachical iron oxide nanocomposites in different fields in Vietnam. However, the achievements are still quite modest compared to other countries in the world. There are still many challenges in the synthesis process as well as in exploring the novel properties of materials that have not been thoroughly researched yet. In recent years in Vietnam, the number of research studies on nanocomposite materials with hierarchical iron oxide structures is still relatively low. Therefore, researching this field has great significance in terms of fundamental science and contributes

to promoting the development of the country. Therefore, we have chosen the topic for our thesis: 'Synthesis, characterization, and application of hierarchical structures iron oxide nanocomposite material'.

2. Research objectives

To study some types of hierarchical structures iron oxide nanocomposites with porosity, in order to understand the nature of material formation and direct the synthesis process, and to control the morphology, structure and size of the material.

Hierarchical structures iron oxide nanocomposite have the ability to catalyze the reduction of 4-nitrophenol as well as exhibit good properties for important applications such as electrochemical sensors for the detection of organic compounds.

3. Research subject and scope

Some types of hierarchical structures iron oxide nanocomposites with defined morphology and high surface area: carbon/α-Fe_2O_3/Ag, Fe_3O_4/Ag, Fe_3O_4/Au. Successfully synthesized materials are applied in the fields of catalysis and electrochemical sensors.

4. Practical significance of the research

The successful synthesis of ordered structure iron oxide nanocomposites with uniform size and high surface area is essential for their application as catalysts in the degradation of harmful organic dyes (4-nitrophenol). In addition, the development of electrochemical sensors with high sensitivity, selectivity, and low detection limits (LOD) can be achieved for monitoring the quality of various types of food and pharmaceuticals. Therefore, this research has practical significance in the fields of environmental protection and food safety.

5. Research novelty

Hierarchical carbon/α-Fe_2O_3/Ag, Fe_3O_4/Au, Fe_3O_4/Ag nanocomposite successfully synthesized were using a hydrothermal method. The characteristic analysis showed that the obtained nanocomposite had a core-shell structure, a well-ordered arrangement, uniform particle size, and a relatively large surface area.

The carbon/α-Fe_2O_3/Ag was used to coated GCE electrode and application for simultaneous voltammetric detection of uric acid, xanthine, and hypoxanthine. The proposed electrotrode exhibited high stability and reproducibility in measurements, with low LOD and satified linear range.

The proposed method based on the Fe_3O_4/Au-GCE electrode represents excellent stability, repeatability, reproducibility for the detection of

chloramphenicol with a low detection limit The proposed sensor demonstrates good performance for CAP electrochemical determination in urine samples.

The Fe_3O_4/Ag2.0 microstructures were used as an electrochemical sensor for detecting 4-NP in water with low LOD and satisfied the linear range. The proposed sensor also exhibited higher stability, repeatability, and reproducibility. On the other hand, catalytic reduction of 4-NP by using Fe_3O_4/Ag2.0 catalysts was performed. The catalytic reduction reaction followed pseudo-firstorder kinetics with high kapp and TOF values.

Chapter 1 Introduction

1.1. Hierarchical structured Iron oxide semiconductor materials

In its natural state, iron-containing compounds mainly include iron oxide, hydroxide, oxyhydroxide, and other related compounds. The primary oxidation state of iron compounds is III, and there are three compounds FeO, $Fe(OH)_2$, and Fe_3O_4 that contain iron in the II oxidation state. Most iron oxides, hydroxides, and oxyhydroxides have defined particle size and crystal structure. Among them, important iron oxides often studied include α-Fe_2O_3 (hematite), γ-Fe_2O_3 (maghemite), and Fe_3O_4 (magnetite). In the 3d orbitals of the Fe atom, there are four unpaired electrons, so they have a strong magnetic moment. When crystals form, Fe atoms can create different states.

Hierarchical structures iron oxide nanoparticles are multidimensional materials that are constructed in an orderly manner from low-dimensional sub-unit nanoparticles such as 0D spheres, 1D rods, 2D sheets, 3D cubes, and so on. In recent decades, there have been many studies related to hierarchical structure iron oxide materials with superior physical and chemical properties compared to other materials. Therefore, they are widely applied in fields such as adsorption, catalysis, and sensors. Hierarchical structure iron oxide nanoparticles have high porosity with diverse morphologies, large specific surface area, rich pore systems, and have enhanced adsorption efficiency, increased contact, adsorption and diffusion of analyte molecules on the electrode surface, leading to fast electrochemical processes and high response. In addition, ordered structure iron oxide materials have a uniform particle size distribution, and less degradation compared to iron oxide nanoparticles with nanosized dimensions. Van der Waals forces between the material particles with ordered structure are relatively weaker than those of nanoparticles with nanostructured bases. Therefore, hierarchical structure iron oxide materials can easily disperse in solvents to form a colloidal solution and can be used as a catalyst carrier. Based on these advantages, hierarchical structure iron oxide materials have received a lot of attention and extensive research in catalysis and sensor applications.

Currently, the classification of iron oxide with hierarchical structures still mainly relies on their natural morphology, such as rod, sheet, or hedgehog-like shape. In addition, the fundamental unit and the existing form of the material's ordered structure are also used to classify and name them. So far, the use of template-based strategies to guide the development of material structures is still considered the simplest and most effective method. The diversity of ordered

structures is built on various fabrication methods, including soft-templating and hard-templating.

1.2. Noble metal nanoparticles (Au, Ag, etc.)

In recent decades, precious metal nanoparticles (Au, Ag, etc.) have attracted the attention of scientific researchers. With excellent optical, electrical, and corrosion-resistant properties, they are considered multi-functional materials and are applied in various fields. In particular, controlling the shape, size, composition, and crystal structure efficiency of precious metal nanoparticles plays an important role in exploring new functions or enhancing their application capabilities in many fields such as catalysis, sensors, and energy. The unique property of precious metal nanoparticles compared to other metals is the surface plasmon resonance property. Currently, there are many methods used to synthesize precious metal nanoparticles, such as chemical, physical, and biological methods. However, for this thesis, the focus is on studying and applying the chemical method to synthesize Ag and AuNPs. Precious metal salt precursors with high oxidation states will be reduced by various reducing agents to form precious metal nanoparticles.

1.3. Hierarchical structured iron oxide nanocomposite

The combination of iron oxide with other phase components such as carbon materials, metal oxides, or noble metals to form ordered structure iron oxide nanocomposites has received wide research attention. This combination is based on dispersing the other phase components on the surface or structure of the single-phase iron oxide to create new and unique physical and chemical properties of the nanocomposites compared to single-phase materials. The diverse shapes and structures of nanocomposite materials are designed by adjusting the phase component ratios in the nanocomposite materials. Generally, the process of synthesizing iron oxide nanocomposite materials is carried out in two steps. First, the nano iron oxide material with a defined shape is synthesized and plays the role of a matrix (primary material). Then, the other phase components are uniformly arranged on the surface or pores of the single-phase nano iron oxide structure to form an ordered structure iron oxide nanocomposite (secondary composite). Currently, two main methods are used to synthesize ordered structure iron oxide nanocomposites, as well as other types of oxide nanocomposites, which are ex-situ and in-situ methods.

Currently, diverse analytical methods have been used to identify inorganic and organic substances. Among them, electrochemical methods utilizing the volt-ampere dissolution technique (ASV) and the volt-ampere differential pulse method (DP-ASV) possess many advantages: high sensitivity and selectivity,

low investment cost... Particularly, in this method, working electrodes developed on the basis of modified nano-electrode materials, such as glassy carbon electrodes, have been extensively researched by scientists around the world. One of the effective approaches to modifying electrodes is to use ordered iron oxide nanocomposites with large effective electrochemical surface area, abundant pore systems, in order to enhance the adsorption and diffusion ability of the analyzed substances on the electrode surface, leading to a fast and highly responsive electrochemical process. The modified metal oxide nanostructure with different phase components demonstrates high selectivity and sensitivity not only from the combination of components but also from creating new properties by the synergistic effect arising from the interaction of the solid surface. In this thesis, iron oxide nanocomposite materials are applied to modify glassy carbon electrodes for analyzing organic substances such as uric acid (UA), xanthine (XT), hypoxanthine (HP), and the antibiotic chloramphenicol. Additionally, iron oxide nanocomposite materials can efficiently catalyze the reduction reaction of 4-nitrophenol.

Chapter 2 Experiment

2.1. Chemicals, equipment, and instruments

The chemicals used in the thesis were purchased from Sigma-Aldrich (USA) and Merck (Germany). Modern equipment was used at industrial university of Ho Chi Minh city, Hue University of Science, and the Vietnam Academy of Science and Technology.

2.2. Procedure

The nanocomposite materials of carbon/α-Fe_2O_3/Ag, Fe_3O_4/Au, and Fe_3O_4/Ag were synthesized using a multi-stage hydrothermal method. The synthesized materials were characterized using various methods such as EDX, XRD, SEM, TEM, HR-TEM, VSM, BET, FTIR, XPS, ICP-OES, UV-Vis, and EIS.

Electrochemical analysis was performed using the von-ampere loop (CVs) and von-ampere stripping voltammetry (DP-ASV) methods to investigate the electrochemical properties of the modified electrodes towards the analyte. The measurements were carried out on a CPA-HH5 Computerizer Polarographic Analyzer (produced by the Institute of Chemistry, Vietnam Academy of Science and Technology), using a three-electrode system consisting of a GCE working electrode with a diameter of 2.8 ± 0.1 mm, an Ag/AgCl/KCl 3M reference electrode, and Pt counter electrode.

The electrochemical impedance spectroscopy (EIS) of the modified electrodes was measured in a $[Fe(CN)_6]^{3-/4-}$/KCl solution with an AC amplitude of 5 mV, an applied potential of 220 V, and a frequency range from 0.1 Hz to 100 kHz using the same instrument mentioned above.

The UV-Vis spectroscopy (Thermo Evolution 201, USA) method was used to investigate the photocatalytic reduction of 4-NP in the presence of catalysts at a wavelength of 400 nm.

CHAPTER 3 RESULTS AND DISCUSSIONS

3.1. Synthesis of hierarchical structured carbon sphere@α-Fe2O3@Ag nanocomposites and their application for simultaneous voltammetric detection of uric acid, xanthine, and hypoxanthine

3.1.1. The formation process of carbon/α-Fe_2O_3/Ag

Fig. 3.1 illustrated the schematic of the formation of carbon/α-Fe_2O_3/Ag. First, α-Fe_2O_3 was self-assembled into the surface of carbon microspheres to form the binary core-shell carbon/α-Fe_2O_3 composite through seed mediated growth method. Eventually, Ag nanoparticles were incorporated into the surface shell layer of the binary Carbon/α-Fe_2O_3 composite owing to the reduction of $NaBH_4$ to produce hierarchically self-assembled carbon/α-Fe_2O_3/Ag ternary core-shell composite.

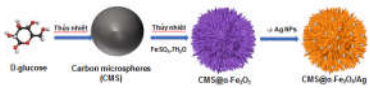


Fig 3.1 Schematic of the formation of carbon/α-Fe_2O_3/Ag.

3.1.2. Characterization

The synthesized carbon exhibited welldefined spheres with a s mooth surface and particle size in the range of 0.2-0.5 μm (Fig. 3.2a). Meanwhile, the obtained carbon/α-Fe_2O_3 and carbon/ α-Fe_2O_3/Ag spheres exhibited a rough (Fig. 3.2b, c). The dot mapping analyses implied that C, O, Fe, and Ag were well-dispersed throughout the carbon/α-Fe_2O_3/Ag sphere.

Crystallographic analyses of carbon, carbon/α-Fe_2O_3 and carbon/α-Fe_2O_3/Ag nanocomposites are shown in Fig. 3.4a. No diffraction peaks were witnessed on the XRD pattern of carbon, suggesting that the prepared carbon had an amorphous structure. On the other hand, the XRD pattern of carbon/α-Fe_2O_3 showed high-intensity peaks at 2θ=24.29, 33.26, 35.83, 40.91, 49.56, 54.08, 62.40, and 64.21°, assigned to the rhombohedral α-Fe_2O_3 (JCPDS card No. 33-0064). Meanwhile, the XRD pattern of the carbon/α-Fe_2O_3/Ag composite exhibited new diffraction peaks of 38.13, 44.31, and 64.31°, attributable to AgNPs (JCPDS card No.04-0783).

Fig. 3.7 compares the oxidation peak currents for UA, XN, and HP with different electrodes, revealing that the fabricated carbon/α-Fe_2O_3/Ag-modified GCE exhibited the highest oxidation peak currents for all components. These findings indicate that the fabricated hierarchical carbon/α-Fe_2O_3/Ag had more excellent electrochemical performance than its counterparts.

Effects of pH media and scan rate on the electrochemical performance that

occurred at the surface of the carbon/α-Fe_2O_3/Ag-modified GC electrode were investigated. Fig. 3.9 shows the CV of UA, XN, and HP on the modified electrode measured at pH=3 to 1, the current for UA, XN, and HP reached the maximum value at pH=7. In addition, their peak potential shifted toward the negative potential area, evidencing the direct involvement of protons in the oxidation process (Figs. 3.9b-c). Fig. 3.9d shows the linear relationship between the anodic peak potential and pH value obtained for UA, XN, and HP, respectively; their corresponding slope values were 0.061, 0.061, and 0.059, respectively. These values were quite close to the Nernst equation, suggesting that the number of protons and electrons involved in the oxidation process on the carbon/α-Fe_2O_3/Ag-modified GCE was equal.

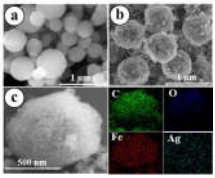


Fig. 3.2 SEM images of (a) carbon, (b) carbon/α-Fe2O3, and (c) carbon/α-Fe_2O_3/Ag, with dot mappings of C, O, Fe, and Ag of carbon/α-Fe_2O_3/Ag sample

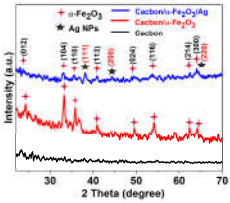


Fig 3.4 XRD pattern of carbon/α-Fe_2O_3 carbon, carbon/α-Fe_2O_3 and carbon/α-Fe_2O_3/Ag.

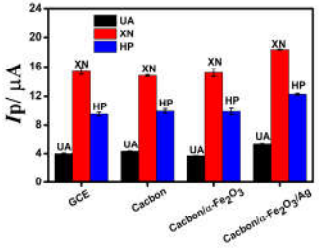


Fig 3.7 The oxidation peak currents of bare GCE, and the GCEs coated with carbon, carbon/α-Fe_2O_3 and carbon/α-Fe_2O_3/Ag in a solution containing UA, XN, and HP (10^{-4} M).

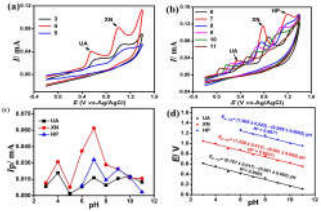


Fig 3.9 Cyclic voltammogram response of CS/α-Fe_2O_3/Ag coated GCE in an equimolar solution of UA, XN, and HP (5×10–4 M) at: (a) pH=3 to 5, (b) pH=6 to 11, (c) the plots of peak currents (I*p*) with pH values, and (d) the linear plots of E*p vs*. pH media*)*.

Upon increasing the scan rate from 0.05 to 0.5 V s^{-1}, the oxidation peak potentials shifted toward the positive area, whereas the anodic peak currents for

UA, XN, and HP increased linearly (Figs. 3.10a-b), suggesting that the oxidation of UA, XN, and HP at the carbon/α-Fe_2O_3/Ag-modified electrode's surface was controlled by the adsorption process. It had been reported that the electrode reaction process was considered to be a diffusion-controlled electrode process when the intercept of the plot for Ip vs. $v^{1/2}$ passed the origin; otherwise, it was an adsorption-controlled process. The plots of Ip vs. $v^{1/2}$ obtained for UA, XN, and HP are shown in Fig. 3.10c, confirming that the reactions of UA, XN, and HP at the surface of the electrode were driven by their adsorption process.

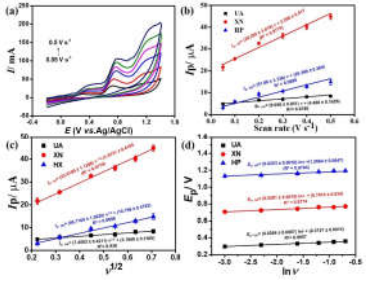


Fig. 3.10 (a) Cyclic voltammogram response of carbon/α-Fe_2O_3/Ag -GCE measured in an equimolar solution of UA, XN, and HP (5×10^{-4} M) at various scan rates, (b) the plots of Ip vs. v, (c) plots of *I*p vs. $v^{1/2}$, and (d) plots of Ep vs. ln*v*.

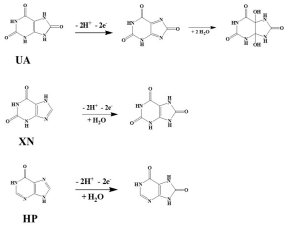


Fig. 3.11 The oxidation reactions of UA, XN, and HP at carbon/α-Fe_2O_3/Ag -GCE

The number of electrons transferred can be determined by employing the Laviron equation. The linear plots of Ep vs. lnv and the corresponding equations obtained for UA, XN, and HP are shown in Fig. 3.10d. For the irreversible process (α=0.5), the numbers of electrons transferred were ~1.944, 1.826, and 2.030 for UA, XN, and HP, respectively, which suggested that two electrons were involved in the redox process. Based on the obtained results, possible mechanisms for the oxidation of UA, XN, and HP at the carbon/α-Fe_2O_3/Ag coated GCE surface are described in Fig.3.11.

Stability and repeatability tests using the prepared carbon/α-Fe_2O_3/Ag-modified GCE were implemented using the DPV method with 0.2-M Britton-Robinson buffer solutions (pH 7). Fig. 3.12 shows the oxidation peak currents observed for the equimolar mixture containing UA, XN, and HP (5×10^{-4} M) during 15 days, revealing a slight decrease of ~10% in peak currents. This finding suggested that the fabricated carbon/α-Fe_2O_3/Ag-modified GCE had good stability. In addition, a series of ten consecutive DPV measurements using the carbon/α-Fe_2O_3/Ag-modified GCE showed that there was only an

insignificant change in their oxidation peak potentials (Fig. 3.13). Differential pulse voltammograms of different equimolar solutions of UA, XN, and HP were recorded to determine the limit of detection (LOD) of the carbon/α-Fe_2O_3/Ag-modified GCE (Fig. 3.14a). The corresponding linear plots of *I*p vs. concentration of the three tested compounds are shown in Fig. 3.14b. LOD is defined as the minimum detectable amount of analyte using the developed electrode, calculated using the LOD=3S/b equation, where S is the standard deviation of the lowest concentration of UA, XN, and HP; b is the slope of the calibration curve obtained from the DPV. Accordingly, the LOD values obtained for UA, XN, and HP at the surface of carbon/α-Fe_2O_3/Ag-modified GCE were found to be ~0.042, 0.089, and 0.048 µmol L^{-1}, respectively.

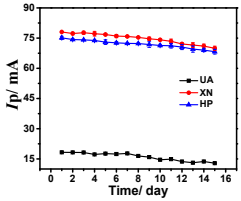


Fig. 3.12 Stability test of carbon/α-Fe_2O_3/Ag-coated GCE measured for 15 days.

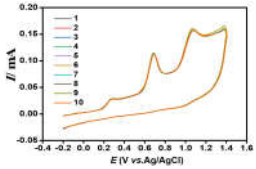


Fig 3.13 Repeatability test of carbon/α-Fe_2O_3/Ag coated GCE10 consecutive DPV measurements.

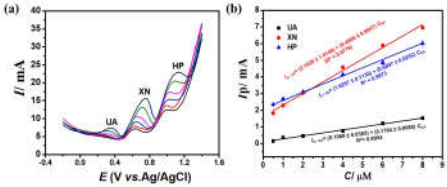


Fig 3.14 DPV in different equimolar solutions of UA, XN, and HP with concentrations ranging from 0.5 to 8.0 µmol L^{-1}, and (a) the plots of anodic peak currents as a function of analyte concentration (b).

3.2. Synthesis of hierarchical flower-like Fe_3O_4/Au nanocomposites and their application for electrochemical detection of Chloramphenicol.

3.2.1. The formation process of flower-like Fe_3O_4/Au

The main stages in the self-assembly process of flower-like Fe_3O_4 porous microstructure can be described as follows. In the initial step, the hydrogen-bonding interaction between glycerol and water forms a homogeneous quasireverse emulsion in the solvent system. In this stage, ferrous ions Fe coodinate with glycerol molecules leading to formation of the Fe-glycerol complexes which aggregate to form nucleation centres and the further crystal growth of ion oxide. At the solvothermal treatment temperature (120 °C), the hydrolysis of the $FeSO_4 \cdot 7H_2O$ precursor occurs with the aid of urea. Simultaneously, the Fe_3O_4 nanoparticles are generated and self-assemble on the surface of the droplets. During the prolonged solvothermal process, these nanoparticles grow to sheet-like nanostructures that intercross to form flower-like Fe_3O_4 porous microstructures. Finally, the quasi-reverse emulsion droplets are easily removed via distilled water and anhydrous ethanol during washing.

3.2.2. Characterization

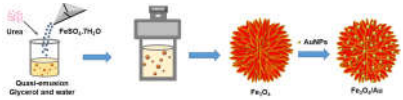


Fig. 3.15. Schematic of the formation of Fe_3O_4/Au.

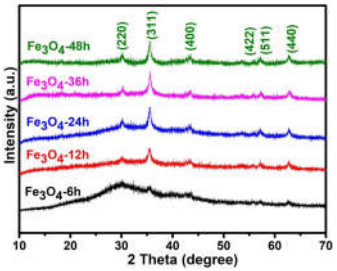


Fig. 3.17 XRD pattern of 3D flower-like Fe_3O_4 porous microstructure synthesized at different hydrothermal reaction times.

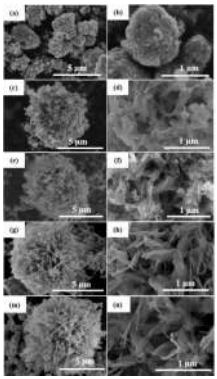


Fig. 3.16 SEM images of the 3D flower-like Fe_3O_4 porous microstructures synthesized at different hydrothermal reaction times: 6 h (a,b), 12 h (c, d), 24 h (e, f), and 36 h (m, n).

The morphological evolutionary process of the Fe_3O_4 porous microstructures at different hydrothermal reaction times (6, 12, 24, 36 h) can be observed from SEM images (Figs.3.16). It was found that the rod-like nanoparticle subunits crystallize into nanosheets that self-assemble to form the 3D hierarchical flower-like Fe_3O_4 porous microstructure during the prolonged hydrothermal reaction (24–36 h).

The crystalline structure of 3D hierarchical flower-like Fe_3O_4 microstructure clearly shows the evolution of the crystallines with the reaction time (Fig.3.17). The diffraction peaks are clearly observed at 2θ of 30.2, 35.5, 43.5, 55.8, 57.1, and 62.3°. These peaks correspond to the diffraction planes (220), (311), (400), (422), (511), and (440) of magnetite Fe3O4 (JCPDS card No. 85-1436). This result indicates that the evolution of the Fe_3O_4 nanoparticle crystalline phase occurs consecutively in the hydrothermal reaction.

The FT-IR spectra provide information about the bonds and groups formed in the molecules composing the material. All the spectra have a similar form (Fig. 3.18), indicating that the Fe_3O_4 microstructure was generated at the early stage of the hydrothermal reaction. The band at 3474 cm^{-1} is attributed to the stretching vibration of the O–H group. The adsorption peaks at 2924 cm^{-1} correspond to the C–H stretching vibrations of the CH_2 group, and the peaks at 1640 cm^{-1} are attributed to the bending vibration of adsorbed water. The absorption peaks at 1395 cm^{-1} and 884 cm^{-1} are assigned to the vibrations of C–C and C–O bonds. These organic components are assigned to the Fe-glycerol complexes which still retains after washing with distilled water and anhydrous ethanol. The formation of Fe_3O_4 is represented by the peaks at 600 cm^{-1} and 423 cm^{-1}, indicating the stretching vibrations of Fe–O at the tetrahedral and octahedral sites.

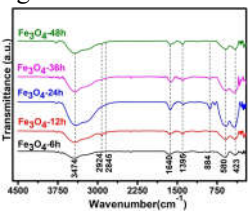


Fig. 3.18 FT-IR spectra of Fe_3O_4 porous microstructure synthesized at different hydrothermal reaction times.

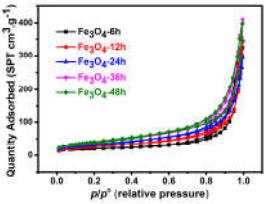


Fig. 3.19 Nitrogen adsorption−desorption isotherms of Fe_3O_4 porous microstructure synthesized at different hydrothermal times

As can be seen in Fig. 3.19, the shape of isotherms at different stages of the hydrothermal process represents the adsorption isotherm of type IV with H3 hysteresis loops, which is characteristic of mesoporous materials. It can be seen

that the calculated BET specific surface area of the as-prepared Fe_3O_4 samples increases significantly from 69.9 $m^2 \cdot g^{-1}$ for 6 h to 117.4 $m^2 \cdot g^{-1}$ for 24 h then slightly to 142.3 $m^2 \cdot g^{-1}$ for 36 and 148.1 $m^2 \cdot g^{-1}$ for 48 h. This can be further confirmed by the development of sheet-like nanoparticle subunits that are interlinked to form porous 3D flower-like Fe_3O_4 microstructure. Thus, the 3D flower-like Fe_3O_4 porous microstructure synthesized at hydrothermal reaction time of 36 h was chosen to be decorated with Au nanoparticles.

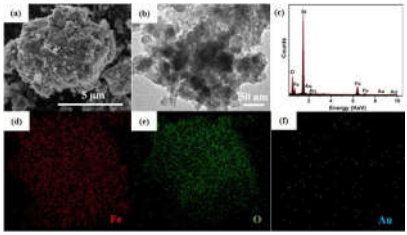


Fig. 3.20 SEM and TEM images (A and B); EDX spectrum (C) and corresponding element mapping images for Fe (D), O (E), and Au (F) of 3D Fe_3O_4/Au porous microstructure.

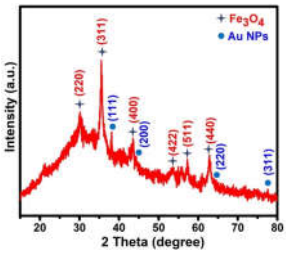


Fig. 3.21 XRD pattern of Fe_3O_4/Au.

The morphology of the Fe_3O_4/Au porous microstructure modified GCE was observed by using SEM and TEM, as illustrated in Figs. 5a, 5b. It is evident that the Fe_3O_4/Au structure presents the porous microstructure composed of interconnected sheet-like nanoparticles that preserve the 3D flower-like porous microstructure morphology. The Au nanoparticles with the particle size of around 10 nm are also clearly identified in the surface of sheet-like Fe_3O_4 nanostructure.

To further confirm the elemental composition of Fe_3O_4/Au porous microstructure, we recorded the EDX spectrum and elemental mapping images (Figs. 3c–3f). The images display the presence and the even distribution of iron, oxygen, gold elements in the Fe_3O_4/Au porous microstructure.

The XRD pattern of the Fe_3O_4/Au porous microstructure is presented in Fig. 6a. Compared with the characteristic diffraction peaks of the as-synthesized Fe_3O_4 in Fig. 3.20, the additional peaks at 38.4, 44.5, 64.7, and 77.5° correspond to the diffraction planes (111), (200), (220), and (311) of Au nanoparticles, respectively (JCPDS card no. 04-0784).

3.2.3. Electrochemical Performance of Different Electrodes

The electrochemical behaviour of unmodified GCE and modified GCE was conducted using CV technique in the absence of CAP (Fig. 3.27a). There were

no any electrochemical signals which are observed at the unmodified GCE while both Fe_3O_4-GCE and Fe_3O_4/Au-GCE exhibit an oxidation peaks at 0.09 V and a reduction peak at -0.60 V. The cathodic peak can be attributed to the reduction of Fe^{3+} to Fe^{2+} and the anodic peak at 0.09 V can be ascribed to the reversible oxidation Fe^{2+} to Fe^{3+}. The cyclic voltammetric studies at bare GCE and modified GCE were performed (Fig. 3.27b). Fig. 3.27c displays the variation of the corresponding peak current response obtained at bare GCE and modified GCE. As can be seen in Fig. 3.27b, a small reduction peak current is observed indicating that GCE exhibits poor electrocatalytic activity towards CAP oxidation. For the Fe_3O_4 modified GCE, anodic peak at 0.025 V in the positive potential scan direction and two cathodic peaks at -0.74 V and -0.08 V in the reserve scan are observed. It is worth noting that the cathodic peak observed at -0.74 V of Fe_3O_4-GCE in the present of CAP is 14 times higher than that of the unmodified GCE (Fig. 3.27c). The enhanced electrochemical sensing ability of CAP at Fe_3O_4-GCE can be attributed the the presence of Fe^{2+} and Fe^{3+} ions in Fe_3O_4. These ions play significantly roles in the electrochemical sensing of CAP throught a rapidly charge-transfer process of Fe^{2+}/Fe^{3+} in the crystal lattice of Fe_3O_4 structure. When the cyclic voltammetric was performed at Fe_3O_4-GCE, the electron was rapidly tranffered between Fe^{2+} and Fe^{3+} ions, leading to form flexible electrons at the surface electrode.

This process can be seen as electrocatalytic activity towards CAP oxidation that enhances electrochemical performance of Fe_3O_4-GCE compared to bare GCE. In addition, the high specific surface of 3D flower-like Fe_3O_4 porous microstructure would provide fast ion transportation for adsorption of CAP in the process of the electrochemical performance. To further verify this properties, the electrochemical behavior of the as-prepared Fe_3O_4-x (x: 6 h, 12 h, 24 h, 36 h, 48 h) modified GCE electrode in 0.1 M B–R BS pH 5.0 containing an equal concentration of 1×10^{-4} M CAP was carried out. The CV curves and the corresponding peak current response were recorded and illustrated in Fig. 3.28. As can be seen in Fig. 3.28, the redox peak currents of the as-prepared Fe_3O_4 samples increases significantly with reaction time from 6 h to 36 h and continous increases slightly with reaction time at 48 h. This can be demonstrated that the specific surface area of the as-prepared Fe_3O_4 samples have significantly effect on the adsorption ability and ectrocatalytic activity towards CAP. For Fe_3O_4/Au-GCE, the highest redox peak currents and lowest potential value compared with other electrodes are observed. The excellent electrochemical behaviour obtained can be attributed to the Au NPs highly dispersed on the 3D flower-like Fe_3O_4 porous microstructure with a large specific surface area. The excellent electron-

conducting tunnel of AuNPs can provide an advantage parthway for electron transfer. Therefore, the synergistic effect of Fe_3O_4 porous microstructure and AuNPs with high electrical conductivity significantly enhances the electrochemical performance towards the sensing of CAP.

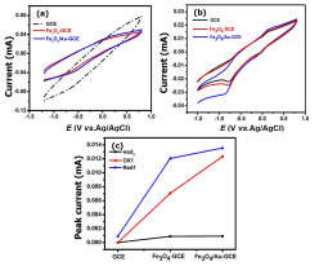


Fig. 3.27 CV curves at GCE, Fe_3O_4-GCE, and Fe_3O_4/Au-GCE in 0.1 M B–R BS pH 5.0 in the absence of CAP (a) and containing 1×10^{-4} M CAP (b). The corresponding peak current response of 1×10–4 M CAP (c)

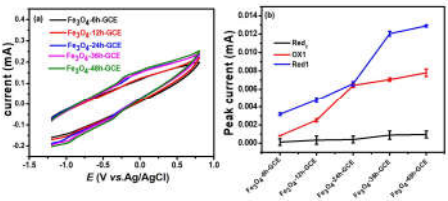


Fig. 3.28 CV curves (a) and the corresponding peak current response of 1×10^{-4} M CAP obtained at bare Fe_3O_4-x modified GCE (b).

The mechanism for the redox process of CAP at Fe_3O_4/Au-GCE was further investigated with the cyclicv oltammetry technique. Fig. 3.29a displays the CV curves recorded with Fe_3O_4/Au-GCE in 0.1 M B–R BS pH 5.0, a scan rate of 100 $mV{\cdot}s^{-1}$ in the presence of 1×10^{-3} M CAP at several scan cycles and Fig. 3.29b presents the relationships between redox peak currents and several scan cycles. In the first scan, upon scanning from negative to positive potentials, a small anodic peak obtained at the potential of 0.025 V (OX1) and a well-defined cathodic peak obtained at –0.74 V (Red1) in the reverse scan. The first reduction peak (Red1) can be attributed to the direct reduction of the nitro group of CAP (–NO2) to the hydroxylamine group of aryl hydroxylamine (–NHOH). This reduction follows a four-electron and four-proton transfer mechanism. In the second cycle, the reduction peak (Red2) at -0.08 V is observed, follow by the decrease in the curent response of peak Red1 and an increase in peak OX1. The oxidation peak at 0.025 V (OX1) and the one at –0.08 V (Red2) are assigned to the reversible reaction of the hydroxylamine group of aryl hydroxylamine (–NHOH) and the nitroso group of nitroso derivatives (–NO) that follow a two-electron and twoproton transfer mechanism. This reversible redox reaction futher increase to the peak at –0.08 V (Red2). It is worth noting that the anodic and

cathodic peak current magnitude stay unchanged during several next cycles, as can be seen in Fig. 3.29b. The proposed electrochemical reaction mechanism is consistent with the results of previous studies, as illustrated in Scheme Fig. 3.30.

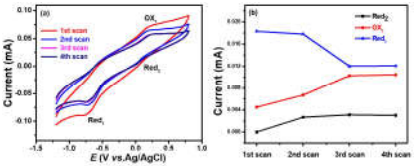


Fig. 3.29 The CV curves of Fe3O4/Au-GCE recorded in 0.1 M B–R BS pH 5.0 in the presence of 1×10–3 M CAP at several scan cycles (a). The relationships between peak current and several scan cycles (b).

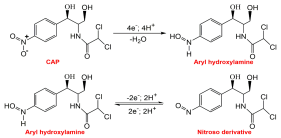


Fig. 3.30 Proposed electrochemical reactions of CAP on Fe_3O_4/Au-GCE.

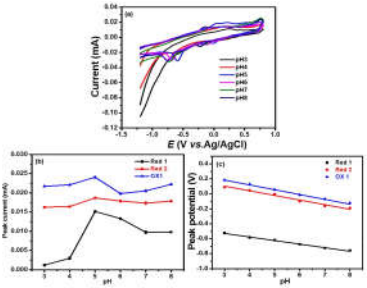


Fig. 3.31 CV curves of Fe_3O_4/Au-GCE in 0.1 M B–R BS containing an equal concentration of 1×10^{-4} M CAP (a); pH dependence of peak current (Ip) (b); linear plot of Ep versus pH (c). Scan rate = 0.1 $V\cdot s^{-1}$

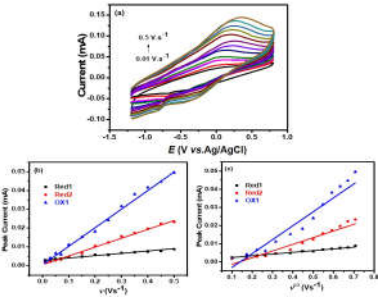


Fig. 3.32 CV curves of Fe_3O_4/Au-GCE (a); linear plot of Ip versus v (b); plot of Ip versus $v^{1/2}$ (c) in 0.1 M B–R BS, pH 5 containing an equal concentration of 1×10^{-4} M CAP at various scan rates.

The electrochemical behaviour of CAP at the Fe_3O_4/Au-GCE electrode can be influenced by the pH value of the electrolyte solution. The CV curves were recorded in the pH range of 3–8 (Fig. 3.31). As shown in Fig. 3.30b, the observed redox peak currents at pH 5 attained a maximal value of 0.015, 0.004 and 0.006 mA, respectively. Therefore, pH 5 was chosen for the electrochemical detection of CAP. The scan rates substantially affect the peak current, and the electrochemical behavior of CAP at the Fe_3O_4/Au-GCE electrode in 0.1 M B–R BS pH 5.0 was carried out with scan rates from 0.01 to 0.5 V.s-1. When the scan

rate increases from 0.01 to 0.5 V.s-1, the cathodic peaks of CAP shift toward the negative values of reduction potential and anodic peak shifts toward the possitive values of oxidation potential. This suggests the electrocatalyst mechanism of the oxidation of CAP where the electrochemical reaction is followed by a homogeneous chemical reaction.

To evaluate the stability, repeatability, the reproducibility of the Fe_3O_4/Au-GCE electrode, we employed the differential pulse voltammetry (DPV) technique in 0.1 M B–R BS at pH 5.0 containing CAP at a concentration of 1×10−5 M.. These indicators prove the suitability of flower-like Fe_3O_4/Au porous microstructure modified GCE for the detection of CAP.

To evaluate the limit of detection (LOD) of CAP at Fe_3O_4/Au-GCE, we recorded the differential pulse voltammetric curves at a concentration varying from 1.0 to 12 µM via the successive addition method. It is noted that the peak current response increases with increasing CAP concentration (Fig. 3.34a). The linear regression equation representing the peak current as a function of analyte concentration is as follows (Fig. 3.34b): Ip (µA)= (0.386 ± 0.017) C_{CAP} + (2.93 ± 0.113), r = 0.995. In this case, the LOD value (3S/b) of Fe_3O_4/Au-GCE is 0.144 µM. The LOD and the linear range values of the proposed Fe_3O_4/Au-GCE in the determination of CAP were compared with those obtained at other modified electrodes (Table 3.2).

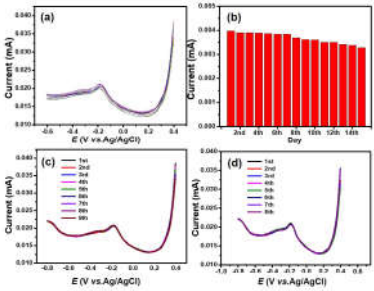


Fig. 3.33 Long-term stability of Fe_3O_4/Au-GCE during 15 consecutive days (a), Repeatability of Fe_3O_4/Au-GCE for 9 consecutive experiments (b), reproducibility of the Fe_3O_4/Au-GCE for 8 times (c).

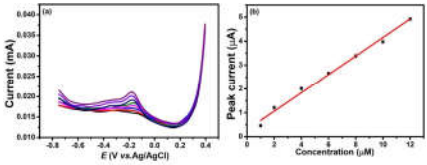


Fig. 3.34 Differential pulse voltammetric curvers at Fe_3O_4/Au GCE in 0.1 B–R BS pH 5 containing CAP at theconcentration varying from 0.2 to 8 µM (a); the plot of peak current as a function of analyte concentration (b).

3.3. Synthesis of hierarchical flower-like Fe_3O_4/Ag microstructure in electrocatalytic detection and catalytic reduction of 4-nitrophenol.

3.3.1. The synthesis process of Fe_3O_4/Ag microstructure

A schematic representation of the reduction process of Ag^+ ions into the pores of Fe_3O_4 is illustrated in Scheme 1. Typically, Fe_3O_4 was initially synthesized through a quasi-reverse emulsion soft template approach using water/glycerol as the reaction media. Then, $AgNO_3$ and NH_3 were introduced into the solution of as-prepared Fe_3O_4. In this step, Ag^+ ions were first reduced by residual –OH functional groups of the Fe(II)-glycerol complexes. These residual functional groups were essential to control the nucleation and uniform immobilization of AgNPs into the pores of Fe_3O_4. The following reactions describe the mechanism for the in-situ reduction reaction of Ag^+ to AgNPs:

$$AgNO_3 + 3NH_3 + H_2O \rightarrow [Ag(NH_3)_2]OH + NH_4NO_3$$

$$-OH^- + 2[Ag(NH_3)_2]OH \rightarrow -(COONH_4) + 2Ag\downarrow + NH_3 + H_2O$$

In the next step, $NaBH_4$ was added to the above mixture for the crystal growth of AgNPs into the pores of Fe_3O_4 microstructure.

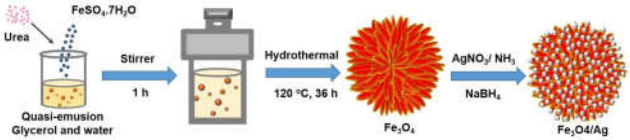


Fig. 3.35 Schematic for the preparation process of Fe_3O_4/Ag microstructure.

3.3.2. Characterization

It can be clearly observed at Fig. 3.36 that the diffraction peaks located at 30.2, 35.5, 43.5, 55.8, 57.1 and 62.3◦ are attributed to (220), (311), (400), (422), (511), and (440) crystal planes of magnetite Fe_3O_4 (JCPDS card No. 85–1436) verifying the formation of Fe_3O_4. For Fe_3O_4/Ag, new diffraction peaks were observed at 38.1, 44.2, 64.4, and 77.3◦ which are attributed to (111), (200), (220) and (311) crystal planes of metallic Ag (JCPDS card No. 04–0783), indicating the existence of AgNPs. UV–Vis spectra of Fe_3O_4 and Fe_3O_4/Agx were recorded to investigate the integration of AgNPs and Fe_3O_4 (Fig. 3.36). The surface plasmon resonance (SPR) absorption peaks for Fe_3O_4/Agx (x = 0.5; 1.0; 2.0; 3.0) were recorded at 376, 379, 367, 474 nm, respectively, compared to Fe_3O_4, demonstrating the successful immobilization of AgNPs. In this case, the absorption peak corresponding to the Fe_3O_4/Ag2.0 appeared at the lowest wavelength (367 nm), indicating the presence of the smallest-sized Ag NPs. Moreover, the absorption peaks of other Fe_3O_4/Agx samples appeared at different wavelengths, demonstrating that the size of AgNPs can be controlled by adjusting the concentration of $AgNO_3$ precursor.

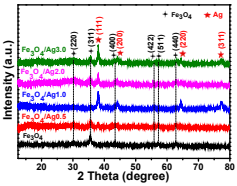


Fig. 3.36 PXRD patterns of 3D Fe_3O_4 và Fe_3O_4/Agx

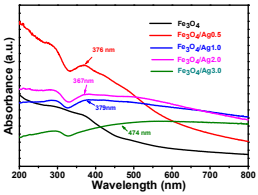


Fig. 3.37 UV-Vis spectra of 3D Fe_3O_4 và Fe_3O_4/Agx

It can be observed that Fe_3O_4 microstructure have a 3D hierarchical flowerlike porous structure with the size of around 400–600 nm. It could be due to the self-assembling of sheet-like nano-subunits (Fig. 3.38). It is worth noting that morphology change was witnessed for the Fe_3O_4/Ag microstructures while varying concentration of $AgNO_3$ precursor.

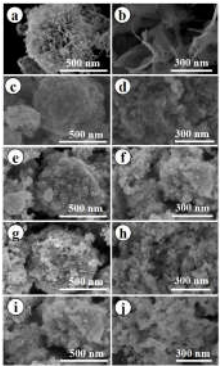


Fig. 3.38 SEM images of Fe_3O_4 (a, b) and Fe_3O_4/Agx (c-j) respectively.

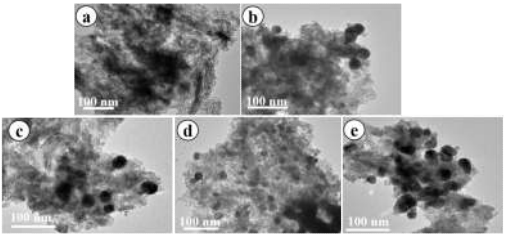


Fig. 3.39 TEM images of 3D Fe_3O_4 (a) and Fe_3O_4/Agx (x=0.5; 1.0; 2.0; 3.0) (b-e).

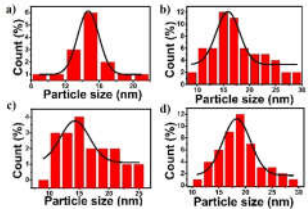


Fig. 3.40 Particle size distribution graphs of AgNPs (a-d) for Fe_3O_4/Agx (x=0.5; 1.0; 2.0; 3.0)

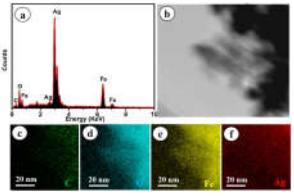


Fig. 3.41 EDS spectra (a), STEM images (b), and Element mapping images for C (c), O(d), Fe (e), Ag (f) of Fe_3O_4/Ag2.0 microstructure.

Transmission electron microscope (TEM) images and corresponding particle size distribution graphs for Fe3O4/Agx microstructures are depicted in Fig. 3.39

and Fig. 3.40. The presence of AgNPs with mean diameters of 14.72 ± 0.01, 15.86 ± 0.37, 14.28 ± 0.80, 18.36 ± 0.26 nm in Fe3O4/Agx-FM (x = 0.5; 1.0; 2.0; 3.0) samples respectively, has been confirmed. EDS spectra showed the presence of carbon (C), iron (Fe), oxygen (O) and silver (Ag) elements in Fe_3O_4/Ag2.0 microstructures (Fig. 3.41a). STEM image of Fe_3O_4/Ag2.0 (Fig. 3.41b) and corresponding element mapping for C, O, Fe and Ag further showed uniform distribution of Ag elements (Fig. 3.41c-f).

3.3.3. Catalytic reduction activity of 4-nitrophenol

The plots for 4-NP reduction reactions in the presence of Fe_3O_4-FM and Fe_3O_4/Agx catalysts are illustrated in Fig. 3.49. 4-NP could not be reduced by using only Fe_3O_4 catalyst. However, 4-NP conversion (83.2, 96.9 and 43.2%) was achieved by using Fe_3O_4/Ag0.5, Fe_3O_4/Ag1.0 and Fe_3O_4/Ag3.0 catalysts, respectively. Moreover, pseudo-first-order kinetics was employed to investigate the kinetics of catalytic reduction reactions. It was found that the *k*app and TOF value for Fe_3O_4/Ag2.0 catalyst was higher than the other catalysts (Fig. 3.50a and b), indicating excellent catalytic reduction activity. Moreover, we investigated the recyclability of Fe_3O_4/Ag2.0 catalyst by using it up to five cycles (Fig. 3.51). In each cycle, Fe_3O_4/Ag2.0 catalyst was collected, followed by washing with deionized water and ethanol before reusing. It was found that the conversion of 4-NP even after 5th cycle was higher than 95%, demonstrating the excellent recycle ability of Fe_3O_4/Ag2.0 catalyst for 4-NP reduction reaction.

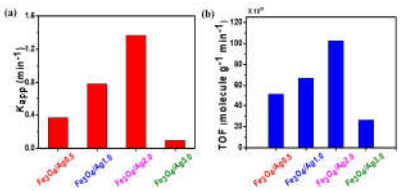


Fig. 3.50 The kapp (a) and TOF values (b) of different catalysts.

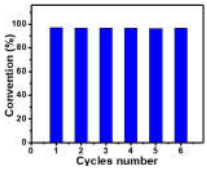


Fig. 3.51 Recyclability of the 4-NP reduction reaction using Fe_3O_4/Ag2.0 catalyst.

3.3.4. Electrochemical Performance of Different Electrodes

The Fe_3O_4/Ag2.0 microstructure was chosen to perform the electrochemical sensor application. The electrochemical performance of bare GCE, Fe_3O_4-GCE and Fe_3O_4/Ag2.0 modified GCE towards 4- NP detection was investigated using the cyclic voltammetry technique. It is worth noting that Fe_3O_4/Ag2.0 modified GCE showed well-defined redox peaks in comparison to bare GCE and Fe_3O_4 modified GCE electrodes: one oxidation peak at 0.22 V and two reduction peaks at −0.59 V and −0.01 V (Fig. 352). Moreover, electrochemical impedance

spectroscopy (EIS) was carried out to further investigate the bare GCE and modified GCE using the ferro/ferricyanide solution as redox probe and Nyquist plot for all electrodes is presented in Fig. 3.52b. The ohmic charge transfer resistance values (Rct) calculated to be 1.44, and 0.35 kΩ for Fe_3O_4 and Fe_3O_4/Ag2.0-FM modified GCE, respectively. These results further demonstrated that small-sized, highly dense and uniformly dispersed AgNPs into the pores of Fe_3O_4 microstructure play a vital role in improving electron transfer kinetic at the electrode-electrolyte interface.

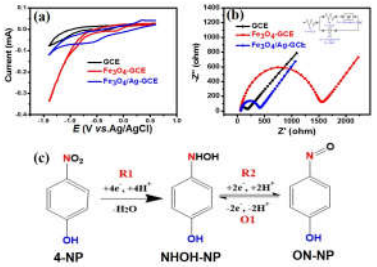


Fig. 3.52 CV curves at bare GCE, Fe_3O_4-GCE, and Fe_3O_4/2.0 modified GCE in 0.1 M BR buffer solutio pH 4.0 (a); Nyquist plot of bare GCE and all modified GCE (b); The schematic of the electrochemical reaction of 4-NP (c)

We further studied the electrocatalytic reaction mechanism for detecting 4-NP at Fe_3O_4/Ag2.0 modified GCE using cyclic voltammetry technique. Accordingly, the plausible mechanism for the electrocatalytic activity of Fe_3O_4/Ag2.0-FM microstructure towards 4-NP detection is illustrated in Fig. 3.52c.

The influence of pH values of electrolyte solution on the electrochemical sensing of 4-NP using Fe_3O_4/Ag2.0 modified GCE was investigated by cyclic voltammetry technique. It was found that pH 4 was chosen as the optimal pH for the electrochemical detection of 4-NP. Moreover, the linear plot of peak potential (Ep) against the pH values is drawn (Fig. 3.54c), and corresponding linear regression equations were defined as follows. It is clearly indicated that the plot values of −0.062 and −0.061 pH^{-1} are equal to 2e− /2H+ for the reversible redox process of the hydroxylamine group (-NHOH) and nitroso derivative group (-NO) respectively. These results demonstrated that the proposed mechanism for 4-NP electrochemical detection using Fe_3O_4/Ag2.0 modified GCE is consistent with the redox process presented in Fig. 3.54c.

Furthermore, the effect of scan rate on the electrochemical behavior of Fe_3O_4/Ag2.0 modified GCE was examined. It was revealed that reduction peak

potentials shift towards negative values and oxidation peak shifts positively on increasing the scan rate from 0.01 to 0.3 V s^{-1}. The linear plots of redox peak current responses against scan rates were drawn (Fig. 3.55), and the corresponding linear regression equations can be described as follows: It is considered that the electrochemical detection of 4-NP is controlled by an adsorption process

The stability, repeatability, reproducibility and LOD of the proposed electrochemical sensor was evaluated by DPV technique. Results confirm that the fabricated Fe_3O_4/Ag2.0 is an efficient electrochemical sensor having high stability, repeatability, reproducibility. The resulting activity could be due to the synergistic effect between the high surface area Fe_3O_4 and good conductive AgNPs. DPV curves for the solutions having a varying concentration of 4-NP (1–15 μM) were recorded, and the corresponding plots of peak current response as a function of analyte concentration was drawn (Fig. 3.58). The peak potential values shift negatively on the increasing concentration of 4-NP (Fig. 3.58a), and the corresponding linear equation, Ip (μA)= (0.209 ± 0.007) C4-NP - (0.691 ± 0.067), (r = 0.995) was expressed in the linear range of 1–15 μM (Fig. 3.58b). Accordingly, the limit of detection (LOD) was calculated to be 0.093 μM.

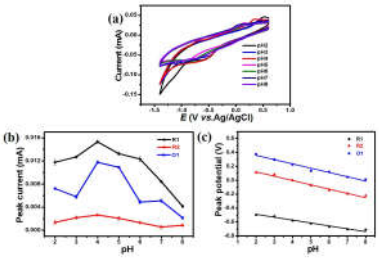
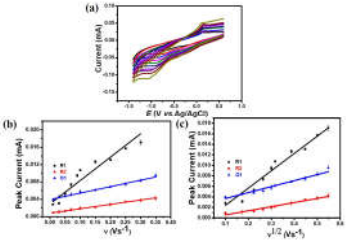


Fig. 3.54. CV curves of Fe3O4/Ag2.0 in 0.1 M BR buffer solution pH 4 at 1 × 10−4 M 4-NP (a); pH dependence of peak current (Ip) (b); the linear plot of Ep versus pH (c).



Hình 3.55. CV curves of Fe3O4/Ag2.0-GCE (d); the linear plot of Ip versus v (e); the plots of Ip versus v1/2 (f) in 0.1 M BR buffer solution, pH 4 at 1 × 10−4 M 4-NP at various scan rates.

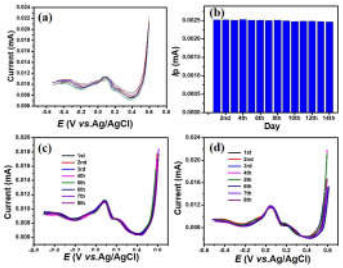


Fig. 3.56 Long-term stability of Fe_3O_4/Ag2.0-GCE (a), Repeatability of Fe_3O_4/Ag2.0-GCE (b), reproducibility of the Fe_3O_4/Ag2.0-GCE (c).

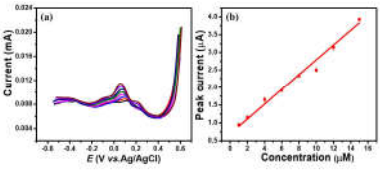


Fig. 3.57 DPV curves at Fe_3O_4/Ag2.0-GCE in 0.1 BR buffer solution pH 4 containing 4-NP at the concentration varying from 1.0 to 15 μM (a); the plot of peak current as a function of analyte concentration (b)

CONCLUSION AND RECOMMENDATION

CONCLUSION

In this thesis, we successfully synthesized hierarchical carbon/α-Fe_2O_3/Ag, Fe_3O_4/Au, Fe_3O_4/Ag nanocomposite using a hydrothermal method. The structural properties were determined by modern analysis methods, including SEM, EM, TEM, Hr-TEM, XRD, XPS, FT-IR, UV-Vis and BET. The characteristic analysis showed that the obtained nanocomposite had a core-shell structure, a well-ordered arrangement, uniform particle size, and a relatively large surface area.

The results showed that the carbon/α-Fe_2O_3/Ag-GCE electrode exhibited high stability and reproducibility in measurements, with a linear range from 0.5 to 8.0 μmol L^{-1} and LOD values of 0.042, 0.089, and 0.048 μmol L^{-1} for the three analytes UA, XN, and HP, respectively. This indicates the potential of this nanocomposite for use in electrochemical sensing applications.

The as-prepared 3D flower-like Fe_3O_4/Au porous microstructure exhibits the characteristics of mesoporous materials with low electrical resistance. The proposed method based on the Fe_3O_4/Au-GCE electrode represents excellent stability, repeatability, reproducibility for the detection of chloramphenicol with a low detection limit of 0.14 μM and the linear range of 1.0 to 12 μM. The proposed sensor demonstrates good performance for CAP electrochemical determination in urine samples.

The Fe_3O_4/Ag2.0 microstructures were used as an electrochemical sensor for detecting 4-NP in water with a LOD of 0.093 μM and satisfied the linear range from 1 to 15 μM. The proposed sensor also exhibited higher stability, repeatability, and reproducibility. On the other hand, catalytic reduction of 4-NP by using Fe_3O_4/Ag2.0 catalysts was performed. The catalytic reduction reaction followed pseudo-firstorder kinetics, and kapp and TOF values were calculated to be 1.36 min^{-1} and 102.35 × 10^{20} molecule $g^{-1}min^{-1}$, respectively.

RECOMMENDATION

The results achieved in this thesis can be a successful first step for us in the process of researching the synthesis of hierarchical structured nanocomposite materials and their applications in catalysis, as well as electrochemical sensors for analyzing organic compounds. In the coming years, we will continue to research and develop the synthesis of nanocomposite materials with hierarchical structures based on other transition metal oxides. The successfully synthesized nanocomposite materials are used as catalysts for the decomposition of organic dyes and electrochemical sensors for identifying other compounds in real samples, such as biological samples and wastewater in aquaculture.

LIST OF PUBLICATIONS

I. Domestic Journal

01. Ho Van Minh Hai, Nguyen Thị Hong Anh, The Ky Vo, Nguyen Quoc Thang, Van Cuong Nguyen (2022), "***Synthesis of hierarchical binary core-branch nanocomposit cacbon microspheres@α-Fe_2O_3 for enhancing electrochemical behavior***", Vietnam Journal of Chemistry (đã được chấp nhận đăng).

2. Hồ Văn Minh Hải, Nguyễn Đức Vũ Quyên, Bùi Thị Hoàng Diễm, Đặng Xuân Tín, Đinh Quang Khiếu, Nguyễn Văn Cường (2022), "**Tổng hợp vật liệu có cấu trúc xốp 3D α-Fe_2O_3 trên cơ sở khung hữu cơ kim loại***", Tạp chí Khoa học và Công nghệ, Trường Đại học Khoa học, ĐH Huế Tập 20, Số 2.*

II. International Journal (SCIE)

01. Ho Van Minh Hai, Dinh Quang Khieu, The Ky Vo, Van Cuong Nguyen, and Jinsoo Kim (2022), "***Synthesis of ternary core-shell cacbon sphere@α-Fe_2O_3@Ag microspheres and their application for simultaneous voltammetric detection of uric acid, xanthine, and hypoxanthine*****",** Korean Journal of Chemical Engineering, DOI: 10.1007/s11814-022-1241-x pISSN: 0256-1115/eISSN: 1975-7220). (Q2, IF=3.309)

02. Ho Van Minh Hai, Dinh Quang Khieu, The Ky Vo, Van Cuong Nguyen (2022), "***Three-Dimensional Hierarchical Flower-like Fe_3O_4 Porous Microstructure Decorated with Au Nanoparticles: Synthesis and Application for Sensitive Electrochemical Detection of Chloramphenicol***", Journal of Electronic Materials volume 51, 5795-5807. (Q2, IF=2.047)

03. Ho Van Minh Hai, The Ky Vo, Thi Hong Anh Nguyen, Dinh Quang Khieu, and Nguyen Van Cuong (2023), **"*Dual role of flower-like Fe_3O_4/Ag Microstructure in Electrocatalytic Detection and Catalytic Reduction of 4-Nitrophenol*",** Materials Science in Semiconductor Processing, Vol 160, 15 June 2023, 107441. (Q1, IF=4.64).

III. Conference

01. Ho Van Minh Hai, The Ky Vo, Dinh Quang Khieu, and Nguyen Van Cuong (2022), Synthesis of hierarchical binary core-shell nanocomposit cacbonmicrospheres@α-Fe_2O_3 for enhancing electrochemical behavior", ICATSD2022, HCM CITY.

02. Ho Van Minh Hai, The Ky Vo, Nguyen Van Cuong (2023), hội thảo khoa học chuyên đề "xúc tác cho sản xuất nhiên liệu", ngày 21-22/4/2023 tại Trường ĐH Duy Tân-TP Đà Nẵng.